Polarforschung 56 (1/2): 43—63, 1986

The North Polar Ice Cap of Mars as a Steady-State System

By W. F. Budd, D. Jenssen, J. H. I. Leach, I. N. Smith and U. Radok*

Summary: The north polar ice cap of Mars is examined with a technique, developed for the ice sheets of Antarctica and Greenland, which rests on the working hypothesis that the mass gain by accumulation on the central part of the ice cap exactly equals the mass loss by ablation from the outer "layered terrain". The movement of the ice is represented by a linear function of the ice thickness which involves in addition the third power of the slowly varying downslope stress and a factor exponentially dependent on the surface temperature. The steady-state assumption then yields the rates of mass gain and loss as the twodimensional divergence of the down-slope mass flux, while the age of the ice is obtained by integration of the velocities along ice flowlines. Since the technique depends on an extrapolation-type estimate of the thickness of the ice-dust deposit, only broad orders of magnitudes of the various features have been obtained at this stage. The inferred movement of the ice reaches maxima of 50 cm horizontally and 2 cm vertically in an earth year, but average values are two orders magnitude smaller. The total inferred mass gain and loss is of the order of 0.2 km³ in a Mars year (1.88 earth years) suggesting that a mass equal to about 20% of the annual atmospheric turnover of water substance, as estimated by JAKOSKY & FARMER (1982), moves through the ice cap over periods ranging from 1 to 100 million (earth) years. These numbers also represent orders of magnitude, at best, since the glaiological analysis involves many unknowns. It can however serve as the starting point for simulating the ice cap changes tha could result from the obliquity cycle of Mars, and especially from the substantially greater insolation of its polar regions associated with an obliquity 10° larger than that existing at present.

Zusammenfassung: Die Eiskappe am Nordpol des Mars wird mit einem Verfahren untersucht, das für die Eisschilde der Antarktis und Grönlands entwickelt wurde und auf der Arbeitshypothese beruht, daß der Massenzuwachs durch Akkumulation im zentralen Bereich der Eiskappe genau gleich ist dem Massenverlust durch Ablation im äußeren „geschichteten" Bereich. Die Bewegung des Eises wird durch eine lineare Funktion der Eisdicke dargestellt, wobei zusätzlich die dritte Potenz der langsam wechselnden, abwärts gerichteten Spannung sowie ein Faktor, der exponentiell von der Oberflächentemperatur abhängt, berücksichtigt werden. Die Annahme eines stationären Zustands liefert dann die Massengewinn- und -verlustraten als zweidimensionale Divergenz des abwärts gerichteten Massenflusses, während sich das Alter des Eises durch Integration der Geschwindigkeiten entlang der Eis-Stromlinien ergibt. Da das Verfahren von einer extrapolationsähnlichen Abschätzung der Dicke der Eisstaubablagerungen abhängt, konnten in diesem Stadium nur grobe Größenordnungen der verschiedenen Erscheinungen bestimmt werden. Die berechnete Eisbewegung erreicht Maxima von 50 cm horizontal und 2 cm vertikal in einem Erdjahr, doch liegen die Mittelwerte zwei Größenordnungen niedriger. Der sich ergebende Gesamt-Massengewinn und -verlust liegt bei 0.2 km³ pro Marsjahr (1,88 Erdjahre), dies bedeutet, daß sich eine Masse von etwa 20% des jährlichen atmosphärischen Wasserumsatzes gemäß der Abschätzung durch JAKOSKY & FARMER (1982) in Perioden zwischen 1 und 100 Millionen Erdjahren durch die Eiskappe bewegt. Auch diese Zahlen sind bestenfalls nur Größenordnungen, da die glaziologische Analyse viele Unbekannte enthält. Die Untersuchung kann jedoch als Ausgangspunkt für eine Simulation der Schwankungen der Eiskappe dienen, die sich aus dem Zyklus der Achsschiefe des Marses ergeben, besonders aus der wesentlich höheren Sonneneinstrahlung auf die Polgebiete des Planeten bei einer um 10° größeren Achsschiefe als der gegenwärtigen.

1. INTRODUCTION

The Mariner and Viking missions to the planet Mars have established that the larger of the two ice caps, located near the north pole and ranging in size between the terrestrial ice sheets of Greenland or West Antarctica and the Vatnajøkul ice cap in Iceland, is made up of water ice with an admixture of dust, alternating in distinct layers. Gravimetric data suggest that the total deposit may amount to $6 \times 10^6 km^3$ or more and that its mean density is around 1 gm cm^{-3} (MALIN, 1986). Various models proposed for the formation of the layers have been reviewed by POLLACK & TOON (1982); the low density seems to favor that of TOON et al. (1980) which sees the dust, representing 5% of the total mass, as becoming concentrated in thin layers between much thicker layers of clean ice. The layers are believed to originate from contrasting climatic epochs produced by changes in the orbital parameters of Mars (CUTTS & LEWIS, 1982), notably a coupled obliquity-eccentricity oscillation with periods of 10^5 and 1.3×10^6 earth years (a) (WARD, 1974).

The layering is believed to hold the most important clues to the nature of the ice cap and has been intensively studied in high-resolution images of ablation troughs located in its peripheral zone (HOWARD et al., 1982; BLASIUS et al., 1982). These troughs are believed to be created primarily by radiation although

* Dr. W. F. Budd, Dr. D. Jenssen and Dr. I. N. Smith, School of Earth Sciences, University of Melbourne, Melbourne (Australia).
Dr. J. H. I. Leach, Division of Geomechanics, CSIRO, Indoorapilly 4068, Queensland (Australia).
Dr. U. Radok, Cooperative Institute for Research in Environmental Sciences, University of Colorado, Boulder CO 80309 (USA).

other factors such as katabatic winds can also play local roles (HOWARD et al., 1982: 204). The possibility of ice flow, on the other hand, has been described as less likely by these authors (HOWARD et al., 1982: 213), who contended that the temperatures are too cold at present to permit flow, and that there is no evidence of crevasses or basal scour features or thinning of layers.

Against this it can be argued that the resolution of layers is imperfect and that the majority of them could be considerably thinner than the resolvable 14-m threshold (BLASIUS et al., 1982: 159); nor would crevasses or scour features be prominent in areas of pronounced ablation and stagnation. Features created by ice flow would be expected to be most prominent in the transition zone between the central unbroken area of the ice cap and its periphery. It is then interesting that in these areas smooth surface undulations with wave lengths of 2 to 10 km have been noted (cf. e. g. Fig. 8 of HOWARD et al., 1982). Such waves are common on terrestrial ice sheets and have been explained by BUDD (1970) as created by ice flow over irregular terrain, accentuating surface wave lengths equal to several times the ice thickness. Finally, the temperatures relevant for ice flow are those deep in the deposit which presumably have been raised well above those of higher layers by the "areothermal" heat flux from the interior of the planet.

We therefore in this paper investigate whether the north polar ice cap of Mars could behave in a manner similar to that of a medium-sized terrestrial ice sheet, after allowing for planetary differences. A particularly interesting possibility is that this might also throw some light on the size of the ice cap and the relative proportions of its major components — the unbroken white interior and the dissected darker peripheral region. As it happens, Mars at present is at a midway stage of the coupled obliquity and eccentricity oscillations. The present size and shape of the north polar ice sheet could therefore approximate a long-term average or nearly steady-state regime.

This working hypothesis suggests the following analysis strategy: Starting from the best available surface elevation patterns the basal topography of the ice cap is inferred from its surface shape and from that of the surrounding ice-free terrain. Ice flowlines are then constructed perpendicular to the surface elevation contours, and ice flow velocities are calculated with a temperature-dependent relation for the deformation of ice under its own weight, derived from laboratory experiments on ice with and without dust inclusions and from measurements on terrestrial glaciers and ice sheets. These velocities make it possible to estimate the distribution and magnitude of the surface mass balance (accumulation and ablation rates) that will keep the ice cap in precisely its present form. The mass balance then defines the vertical velocities in the ice, and both the age and residence time of the ice in different parts of the ice cap.

Building on these time-independent results we finally discuss the possibility of reconstructing ice sheets that might have existed on Mars at opposite extremes of the 10^5 ka obliquity cycle and given rise to the extensive "layered terrain" (DZURISIN & BLASIUS, 1975) believed to form the present ice cap.

2. A MODELLING STRATEGY

The assumption that an ice cap is in a state of zero net mass balance ("balance") reduces the equation of continuity to the form

$$\nabla \cdot (V_b Z) = A - M \qquad (1)$$

Here Z is the ice thickness (difference between the surface elevation E and bedrock elevation B), V_b is a vertically averaged ice velocity, A is the rate of accumulation ($A > 0$) or ablation ($A < 0$), and M is the rate of basal melt (negative for accretion). For terrestrial ice sheets the information existing for Z and A permits equation (1) to be solved for V_b, the "balance velocity" (see. e. g. BUDD et al., 1970) by assuming in the first place that M is negligible; this needs to be confirmed by thermodynamic calculations.

On earth the basic assumption of balance can then be tested by comparing V_b with observed velocities or with a "dynamic" velocity derived from the flow law of ice,

$$\bar{V} = k\tau_b^3 Z \tag{2}$$

Here τ_b is the downslope or basal shear stress, given by $\tau_b = \varrho\, g\, Z\, \alpha$, where ϱ is the ice density (910 kg m^{-3}), g is the acceleration of gravity (9.81 m sec^{-2} on earth, 3.72 m sec^{-2} on Mars), and α is the magnitude of the surface slope, $|\nabla E|$. Since the slope and the ice thickness vary in opposition to one another, τ_b is a slowly changing quantity. The factor k depends primarily on temperature and has the form $k = \exp(a\,T - b)$ where the values of the constants a and b depend somewhat on the crystal structure of the ice, its content of impurities, etc. T is a representative temperature for the lower ice layers which undergo the main shear. For terrestrial ice sheets it has been calculated by integrating the equation of temperature conduction

$$\frac{\delta T}{\delta t} + V\frac{\delta T}{\delta x} - w\frac{\delta T}{\delta z} = \varkappa\frac{\delta^2 T}{\delta z^2} \tag{3}$$

This involves in addition to the thermal diffusivity ($\varkappa = K(c\varrho)^{-1}$ where K ist the conductivity and c the heat capacity of the ice), the heat advection both along the ice flowline $\left[V\frac{\delta T}{\delta x}\right]$ and along the vertical $\left[w\frac{\delta T}{\delta z}\right]$. However, when V and w are small, as in the case of Mars, (3) reduces to the simple steady-state form

$$\frac{\delta^2 T}{\delta z^2} = 0 \tag{3'}$$

which has the solution

$$T = T_s + \gamma z$$

where γ is the thermal gradient created by the upward heat flux from the interior of the planet, and T_s is the temperature in the surface layer below the depth of appreciable annual variations (approximately 10 m).

For the north polar ice cap of Mars, only E and T_s are known, albeit imperfectly, from the Mariner and Viking measurements. The modeling strategy that will be adopted here consists of inferring first of all the ice thickness $Z = E - B$ from the measurements of E and from a hypothetical bedrock topography B, constructed as a smooth continuation of the ice-free topography surrounding the ice cap below its interior. The base stress τ_b can then be calculated, and together with the representative temperature T (further discussed in section 6) leads to estimates for the dynamic velocity $\bar{V} \approx V_b$. Finally equation (1) is solved for the total mass balance $A - M = \nabla\cdot(\bar{V}Z)$. M in the first place can be assumed to be negligible; a check of this assumption is made in section 6.

To complete the description of the ice cap, the total mass flux is obtained as the integral of A over the accumulation area, or alternatively as the integral of $\bar{V}Z$ along the boundary between the accumulation and ablation areas. The vertical and horizontal displacements of an ice particle define its trajectory through a flowline cross section of the ice cap. Using the subscript x for values at position x along a flowline, the particle position x', z' in the ice cap at time t after its deposition on the surface is given by

$$z' = \int_0^t A_x\frac{Z_x - z}{Z_x}\,dt \quad \text{and} \quad x' = \int_0^t \bar{V}_x\,dt \tag{4}$$

while the age of the ice at that position is found as

$$t = \int_0^{x'} dx/\bar{V}_x \tag{5}$$

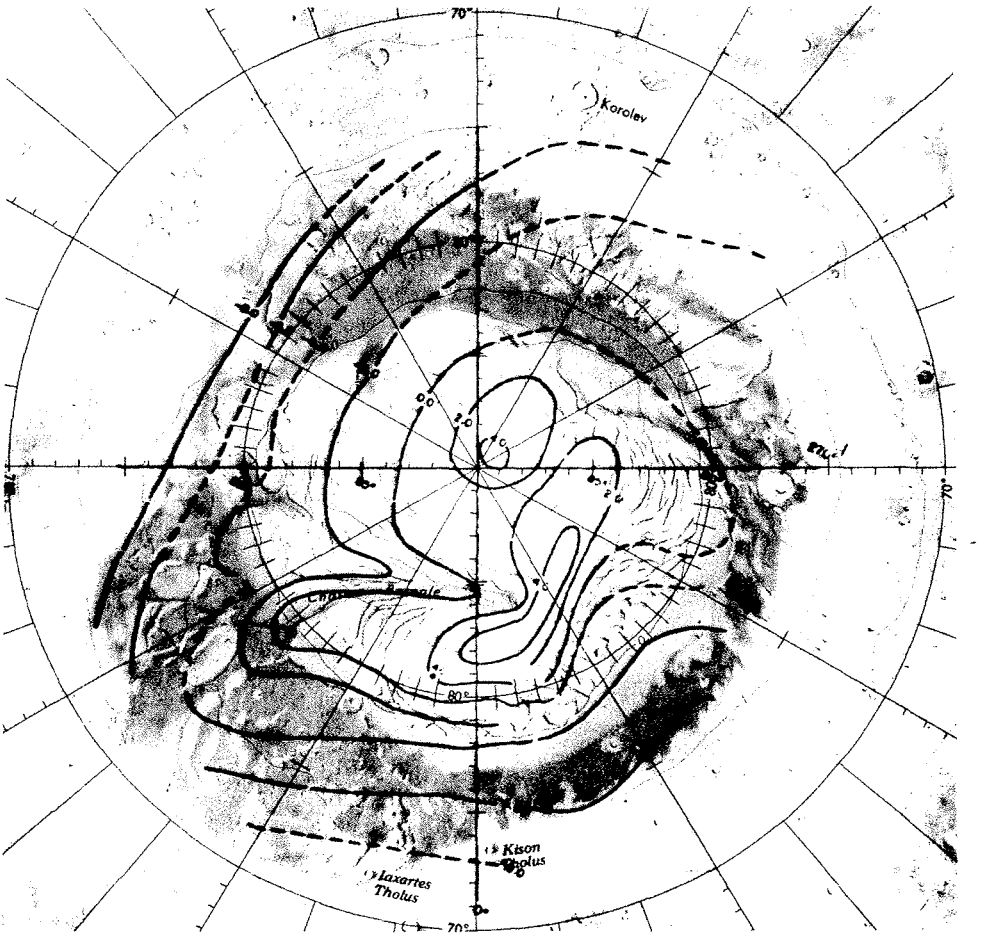

Fig. 1: Surface elevation contours (km) of the north polar region of Mars (DZURISIN & BLASIUS, 1975) superimposed on USGS Map I-961.

Abb. 1: 1 km-Höhenlinien der Oberfläche der nördlichen Polarregion des Mars, überlagert der USGS-Karte I-961 (DZURISIN & BLASIUS 1975).

The "residence time" remaining for the ice at any point in the ice cap is found by deducting its age at x′, z′ from the age t_f of the trajectory end point in the ablation zone:

$$R = t_f - t = \int_t^{t_c} dx/\bar{V}_x \qquad (6)$$

The computational details are set out in the appendix; thermodynamic aspects are discussed in section 6.

3. BASIC DATA

A first photogrammetric model of the north polar ice cap of Mars was constructed from Mariner data by DZURISIN & BLASIUS (1975) and is shown in Fig. 1 superimposed on part of map # I-961 of the U. S. Geological Survey. Pending the completion of a more precise recalculation with the Viking data (SHERMAN WU, pers. communication) these elevation contours were digitized as one of two basic data sets for

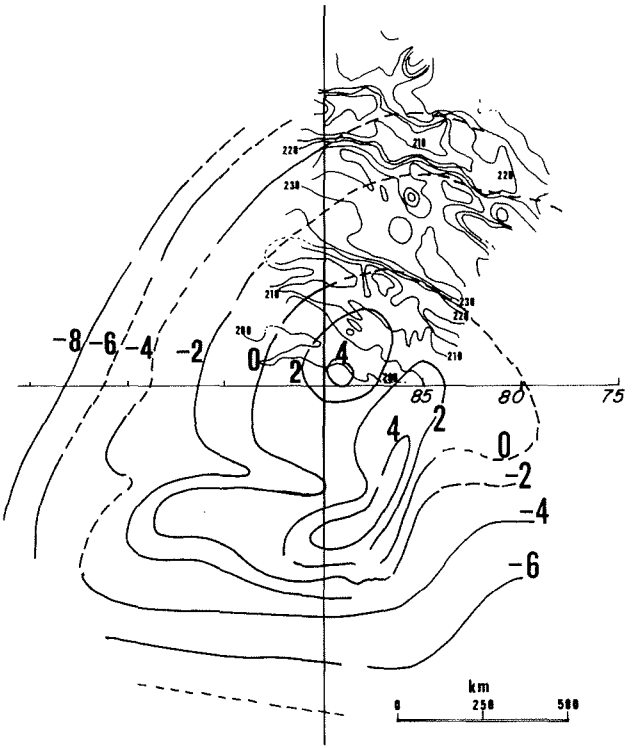

Fig. 2: Surface elevation (km) contours (DZURISIN & BLASIUS, 1975, heavy lines) and surface isotherms (°K, KIEFFER et al., 1977, thin lines).

Abb. 2: 1 km-Höhenlinien der Oberfläche (DZURISIN & BLASIUS 1975, dicke Linien) und Isothermen an der Oberfläche (° K, KIEFFER et al. 1977, dünne Linien).

the present study. It is interesting that the height difference between the ice cap summits and the surrounding terrain is similar to that between the top of the Antarctic ice sheet and the bed of the surrounding ocean.

The other data are surface temperatures derived by KIEFFER et al. (1977) for one occasion and for a segment of the ice cap from Viking measurements during the northern summer (Fig. 2). Bands of rapid temperature changes are indicated near the edge of the ice cap where the elevation also is highly variable. Over its interior, surface temperatures vary from —70 to —50° C in summer, as compared with simultaneous winter temperatures around —130° C over the southern ice cap. For the model calculations annual mean temperatures are needed; they can therefore be assumed to range from around —100° C on the highest parts of the northern ice cap to around —60° C at levels up to 8 km lower near its borders.

Although the surface albedo dominates the surface temperatures in summer, the detailed pattern of the annual mean surface layer temperature probably depends mainly on elevation, as is the case for the terrestrial ice sheets. The rate of vertical temperature change along terrestrial ice cap surfaces ("topographical lapse rate") has been discussed by JENSSEN & RADOK (1982); it approximates the dry adiabatic value $\Gamma = g/c_p$ where c_p is the specific heat for constant pressure. In the case of Mars, this has the value 0.83 J $g^{-1}K^{-1}$ for CO_2, (cf. e. g. GOODY & WALKER, 1972, Tab. 3.2) giving $\Gamma = 4.5°$ K km^{-1}. The total temperature change near the edge of the ice cap in Fig. 2 can be seen to be of the order of 20° K, compatible with elevation changes of the order of 4 km, whereas in the free lower troposphere of Mars the temperature has been found to decrease on the average at the rate of 2.5° C/km (KONDRATYEV & HUNT, 1982). These numbers provide a close analogy to those found on earth (adiabatic lapse rate 10° C/km, mean lapse rate 5.5° C/km) and suggest that similar dynamic and thermodynamic processes involving both the local heat balance and advection may be at work over the polar ice sheets of both planets. For

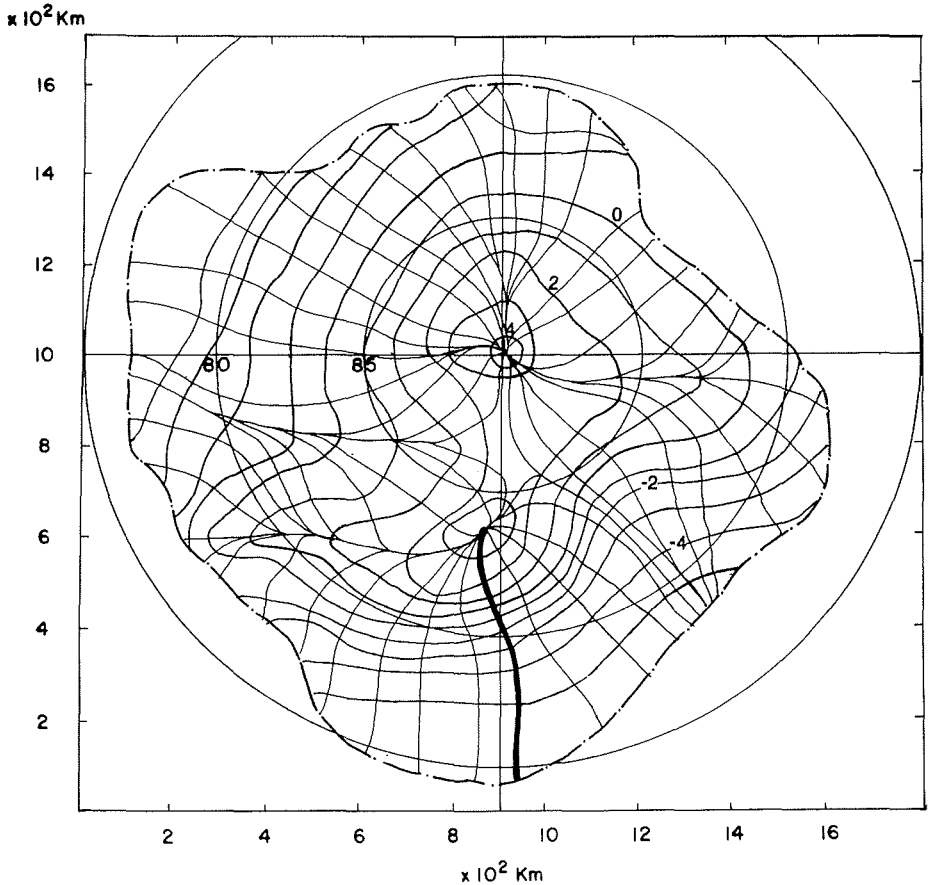

Fig. 3: Surface elevation (km) contours (redrawn from a digitization of the contours in Fig. 1) of the north polar ice cap, and orthogonal ice flowlines. The heavy line marks the cross section of Figs. 11 and 12.

Abb. 3: 1 km-Höhenlinien der Oberfläche (rekonstruiert aus einer Digitalisierung der Höhenlinien in Abb. 1) der Eiskappe am Nordpol und orthogonale Eis-Stromlinien. Die verstärkte Linie kennzeichnet das Querprofil der Abb. 11 und 12.

the present purpose the annual mean surface layer temperature therefore should be representable in first approximation as a single linear function of the surface elevation.

4. PHYSICAL CHARACTERISTICS OF THE ICE CAP

4.1 *Basic Variables*

The main features of the ice cap surface topography, as reconstituted from the digitization of Fig. 1, are two domes denoted by A and B, rising 3.6 km over the surrounding ice-free terrain (Fig. 3). The ice flow on scales exceeding several times the ice thickness can be assumed as outward and orthogonal to the surface elevation contours. Such ice flowlines are indicated in Fig. 3, where the heavy line marks the cross section to be discussed in detail below (section 5).

By inference from terrestrial analogues, the surface domes should reflect the existence of similar and more pronounced features in the bedrock topography. This was taken into account in the construction of key cross sections by an inward extension of the ice-free surroundings of the ice cap (Fig. 4). The bedrock

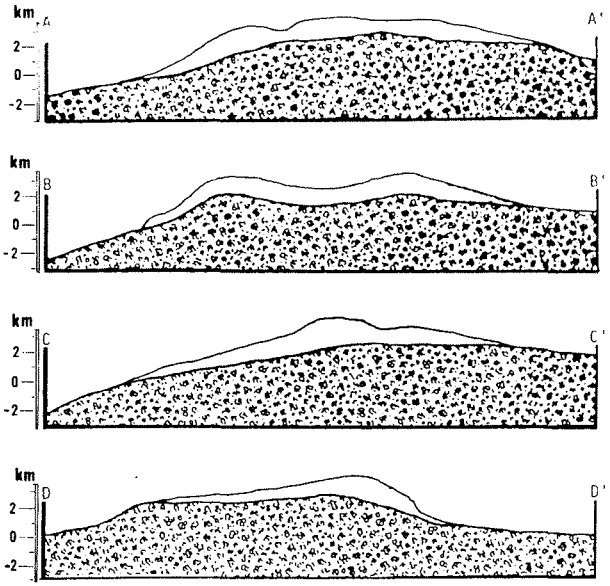

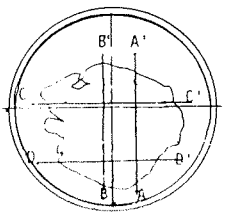

Fig. 4: Cross sections through the ice cap, used to construct the bedrock topography by interpolation from the surrounding ice-free terrain.

Abb. 4: Querprofile durch die Eiskappe zur Konstruktion des Untergrundreliefs durch Interpolation aus dem eisfreien Gelände der Umgebung.

topography composed of such cross sections is shown in Fig. 5, and its subtraction from the elevations in Fig. 3 has yielded the isopleths of ice thickness (Fig. 6). Since the ice thickness is a key parameter in the ice flow relationship (2) it is essential to provide independent arguments supporting the view that the thickness values in Fig. 6 could have the right order of magnitude.

One such argument can be based on the horizontal extent of the ice cap. The maximum thickness of an isostatically adjusted ice sheet of half-width L with plastic rheology, according to WEERTMAN (1976), is $h = (12\tau\varrho g)^{1/2} L^{1/2}$. Here τ is the yield stress (10^5 Pa, say, for Martian temperatures), ϱ is the density of ice (910 kg m^{-3}), and $g = 3.7$ m sec^{-2} is the acceleration of gravity on Mars. For $L = 500$ km this gives a maximum thickness of 4 km. A slightly smaller but comparable value has been found by KRASS (1985) for a model with visco-plastic rheology (KRASS, 1983).

A further feature supporting a maximum ice thickness of that order of magnitude is the surface undulations on the ice cap which have been described by CUTTS et al. (1979) and HOWARD et al. (1982). These undulations closely resemble those commonly found on terrestrial ice sheets. Following BUDD (1970), BUDD & CARTER (1971) and BUDD & YOUNG (1979) have shown that the undulations are created by the flow of the ice over irregular bedrock, and that the length of the resulting surface waves tends to be of the order of several times the ice thickness. The undulations reported by CUTTS et al. (1979) included relatively smooth waves (cf. their Fig. 7, p. 2985) as well as criss-cross arcate undulations which they called an "egg-carton" topography. The latter is also rather common on terrestrial glaciers and ice sheets with divergent curved flow. The smooth Martian surface waves have lengths of the order of 8—10 km; they therefore point to ice flow and to thicknesses of the order of 3—4 km as potentially responsible mechanism, with differential ablation as a subsequent and increasingly important factor, as the ice stagnates in the outer region of the ice cap. The relatively smooth surface and the complete absence of craters in the interior of the ice cap also could be an indication of thick ice which can flow and accumulate to fill in any large indentation.

4.2 *Derived Characteristics*

Surface slopes have been obtained as vector gradients of the surface elevation, ∇E. They increase outward from the two domes and reach maxima at some distance from the edge of the ice cap. In conjunc-

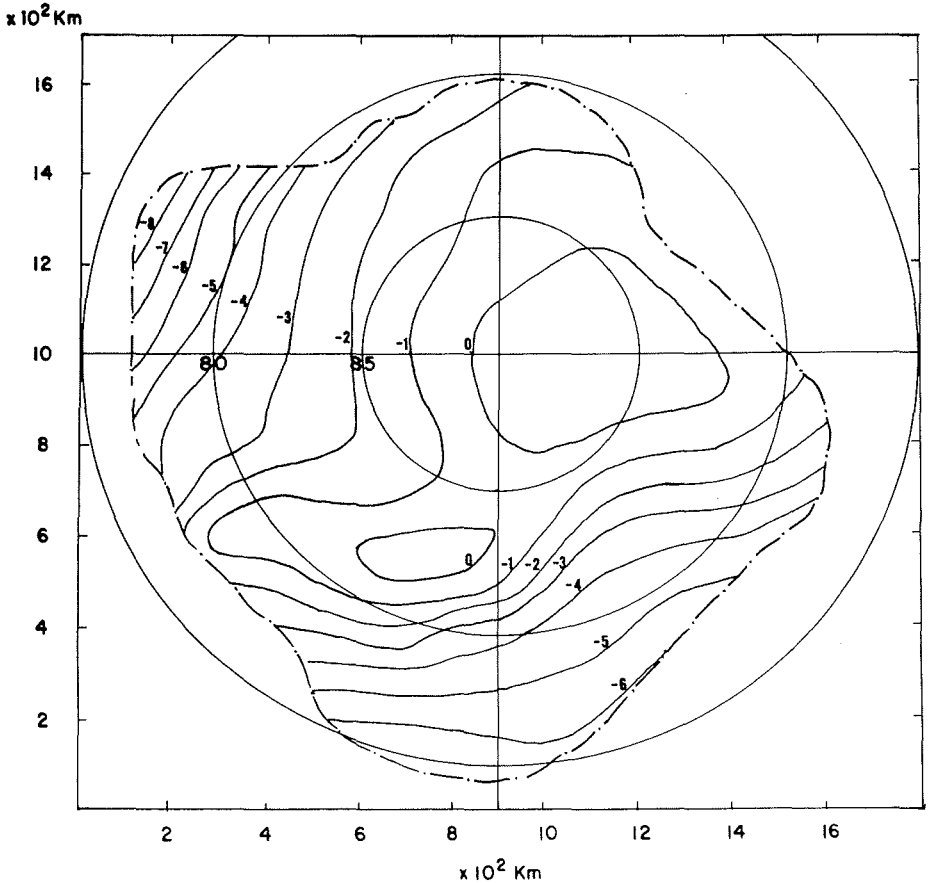

Fig. 5: Bedrock elevation B (km) contours inferred from the cross sections of Fig. 4 and surface features.

Abb. 5: 1 km-Höhenlinien des Untergrundes B, abgeleitet aus den Querprofilen der Abb. 4 und Erscheinungen an der Oberfläche.

tion with the ice thickness (Fig. 6) the slopes produce basal shear (and downslope driving) stresses $\tau_b = g\varrho Z\nabla E$ as large as those found in terrestrial ice sheets, 10^5 Pa.

In order to translate these thicknesses and stress values into ice velocities it can be assumed that the main ice deformation takes place in the deeper layers of the ice-dust deposit where the temperatures are some 20 °C higher than at the surface (cf. section 6). Combining τ_b, Z, and the temperature-dependent factor k in the velocity relation (2) yields the quasi-horizontal "dynamic" velocity $\bar{V}$ shown in Fig. 7. Its most prominent feature is the region of fast flow down the southern dome where the calculated velocities reach extreme values of the order of 50 cm a^{-1}. Over the remainder of the ice cap more typical velocities are two orders of magnitude smaller and drop to fractions of m a^{-1} in the flat and thin outer regions of the ice cap.

The velocities of Fig. 7 when multiplied by the ice thicknesses of Fig. 6 define the horizontal mass flux ϕ: its major features are shown in Fig. 8. The regions of maximum flux near the two domes mark the position of the equilibrium line between the areas with net accumulation and net ablation which can be determined along each flowline and is shown by the dash-dot line in Fig. 8. The line integral of the ice cap mass flux, $\int \bar{V}Z\, ds$ along that line equals the total annual accumulation on the ice cap and, in the state here as-

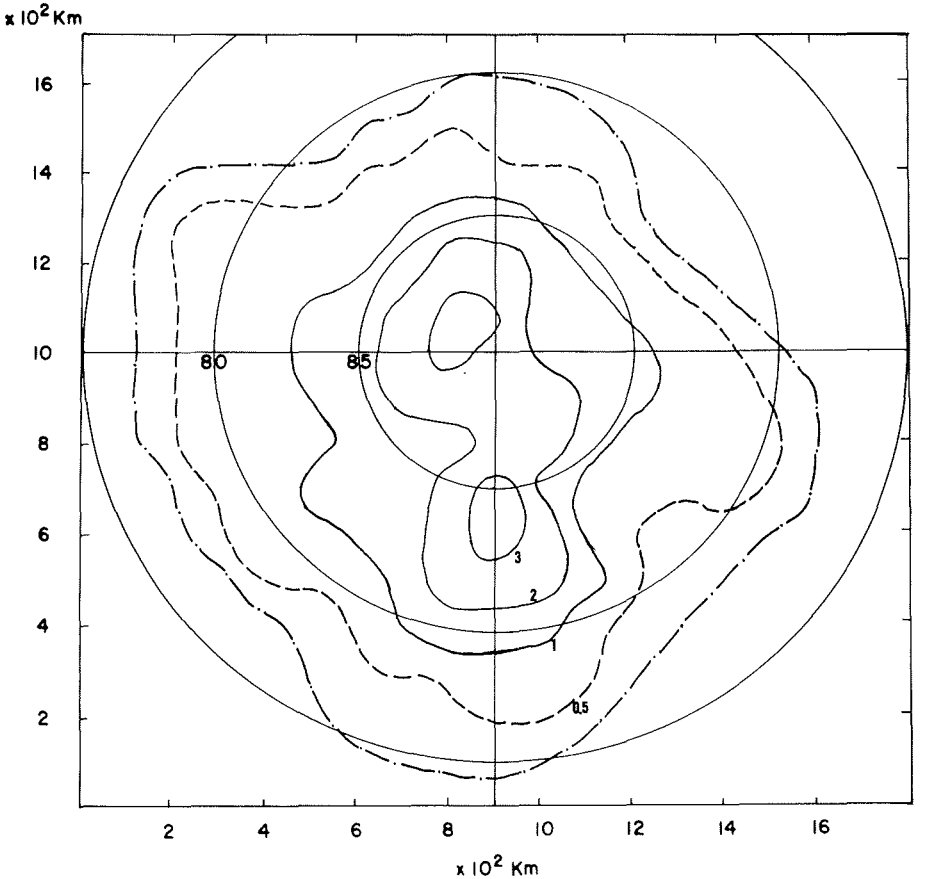

Fig. 6: Ice thickness (Z km) isopleths obtained by subtracting Fig. 5 from Fig. 3.

Abb. 6: Linien gleicher Eisdicke Z in km, gewonnen als Differenzen zwischen Abb. 5 und Abb. 3.

sumed, also balances the total net ablation over its low outer regions. It should be remembered, however, that a possible mass balance contribution from basal melt is disregarded here and in what follows. The potential errors are considered in section 6 below.

The detailed accumulation/ablation fields have been computed from the divergence of the complete set of grid point mass flux values and are shown in Fig. 9. The maxima of net accumulation are found near the two domes; that of the southern dome is adjacent to an area of marked net ablation. In these small areas of high mass balance values of the order of ± 2 mm a^{-1} are suggested by the model simulation. Observational support for the broad pattern of accumulation and ablation is provided by the fact that the boundary between the accumulation and ablation areas is in good agreement with the transition from the residual white region at the end of summer to the more dissected region of the "layered terrain" where ablation tends to concentrate and reveal the dust deposited with the ice.

Without basal melt the total accumulation and ablation are found by integration to amount to 0.11 km^3a^{-1} or 0.20 km^3 of ice during a Mars year. Such an average long term quasi-steady mass flux through the ice cap seems not unreasonable by comparison to the amount of water transported from the summer to the winter hemisphere and back during a Mars year in the atmosphere, 1 km^3 (JAKOSKY & FAR-

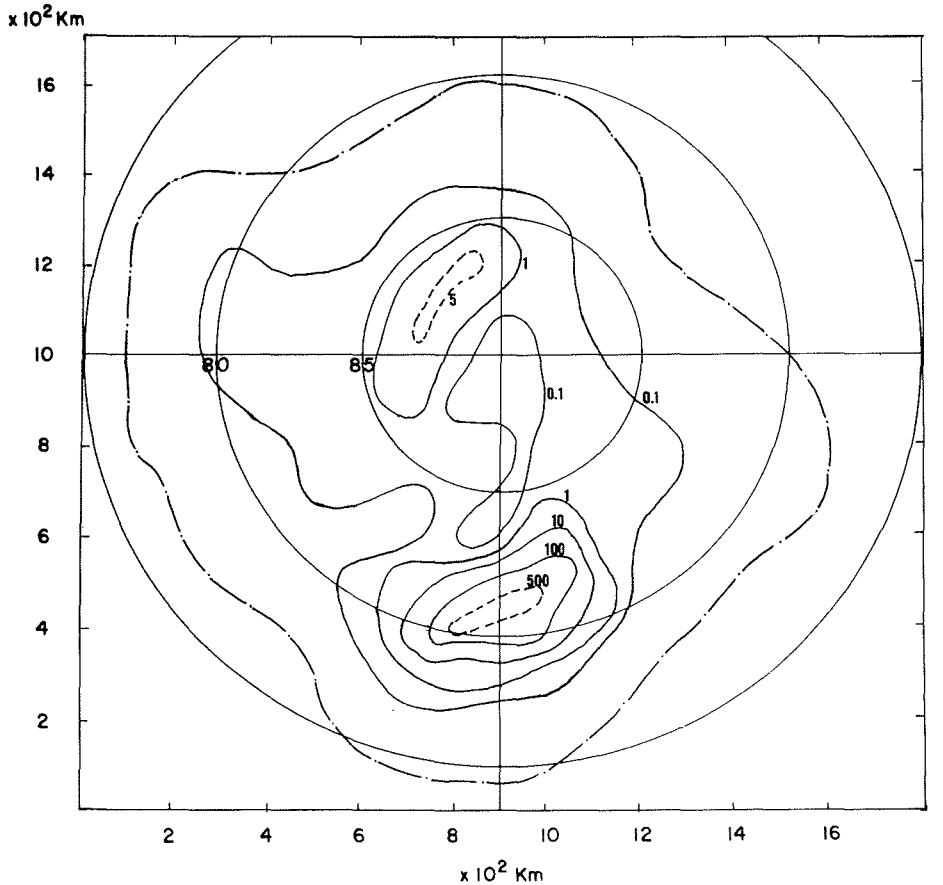

Fig. 7: Isotachs (mm a^{-1}) of the horizontal ice velocity averaged over depth $\bar{V} = k(T)\tau_b^3 Z$. For explanation see text.

Abb. 7: Linien gleicher Horizontalgeschwindigkeit (mm a^{-1}) des Eises, gemittelt über die Tiefe $\bar{V} = k(T)\tau_b^3 Z$. Erklärung im Text.

MER, 1982). Much of this is believed to come from sources other than the ice cap, such as the regolith.

The calculated average accumulation rate on the ice cap works out at 0.27 mm ice a^{-1} and the ablation rate at 0.09 mm a^{-1}. These values are of the same order of magnitude as the estimates of POLLACK et al. (1979, p. 2943) based on atmospheric measurements which suggested an average sedimentation rate of 4 x 10^{-2} g cm^{-2} a^{-1} of a 50% dust-ice mixture, corresponding to the addition of a 0.4 mm thick layer in the polar region of Mars during an earth year (see also FARMER & DOMS, 1979).

The mass balance field of Fig. 9 provides the interface between the glaciological arguments here presented and the extensive work on Martian atmospheric processes. To complete the present glaciological analysis it remains to consider the internal characteristics of the ice cap that are implied by the computed velocity and mass balance fields and by the surface temperatures.

5. THE ICE CAP INTERIOR

With the basic steady-state assumption of the ice cap model, the accumulation and ablation rates repre-

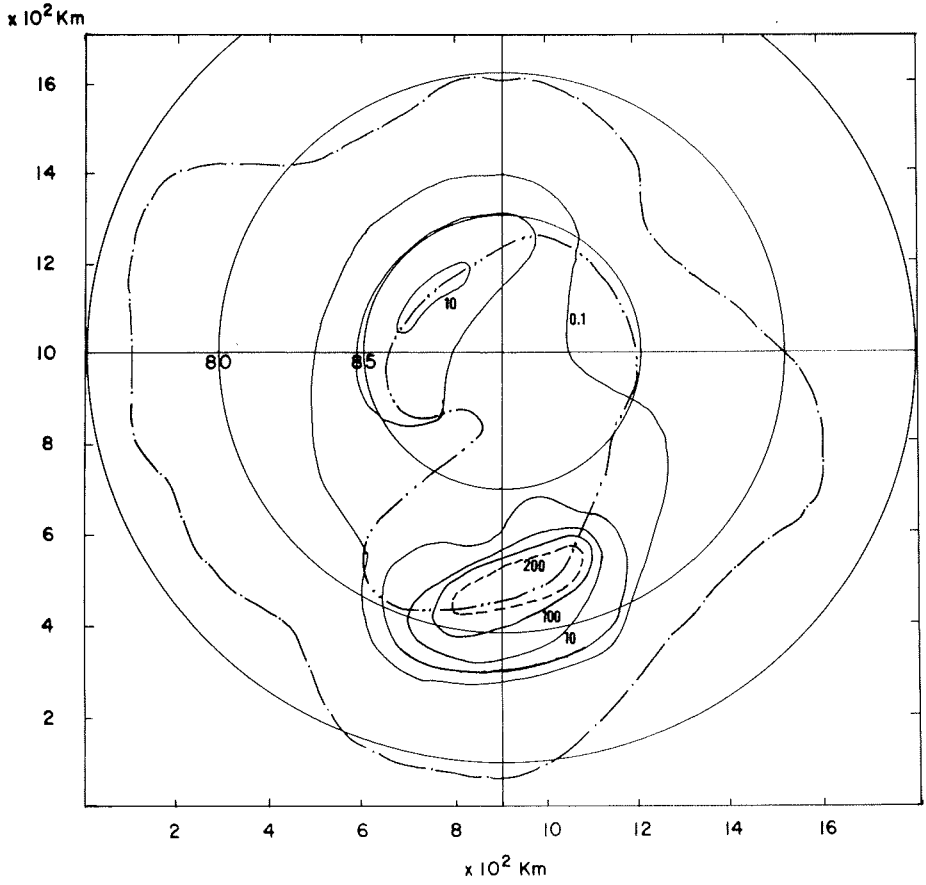

Fig. 8: Volume flux $\bar{V}Z$ (m^3/m a). The line _..._..._ separates the regions with surface accumulation and surface ablation (cf. Fig. 9).

Abb. 8: Massenfluß $\bar{V}Z$ in m^3/ma. Die Linie _..._..._ trennt die Gebiete mit Akkumulation an der Oberfläche von denen mit Ablation (s. Abb. 9).

sent the vertical velocities w_o at the ice cap surface. Inside the ice the vertical velocity depends on further assumptions concerning the vertical strain rate $\dot{\epsilon}_z = \partial w/\partial z$. In the simplest case $\dot{\epsilon}_z$ = const. and

$$w_z = A \frac{Z-z}{Z} \tag{7}$$

where z is the depth below the surface. A more realistic formulation due to BUDD et al. (1976) reduces the vertical velocity at some level $\xi = Z - z$ above the bed in proportion to the horizontal mass flux below that level, i. e.

$$w_\xi = A \frac{\xi \bar{V}_\xi}{Z \bar{V}_Z} \tag{7'}$$

where the overbar now denotes an average over the height indicated by the subscript. When used in equation (6) for the age of the ice, equation (7') gives smaller ages than equation (7) for the surface layers and larger ages for the basal layers of the ice cap. The limited data available for Mars do not warrant the distinction between (7) and (7'). The order of magnitude calculations of ages, residence times and internal temperature have therefore been carried out with (7) for the cross sections along the flowlines in Fig. 3.

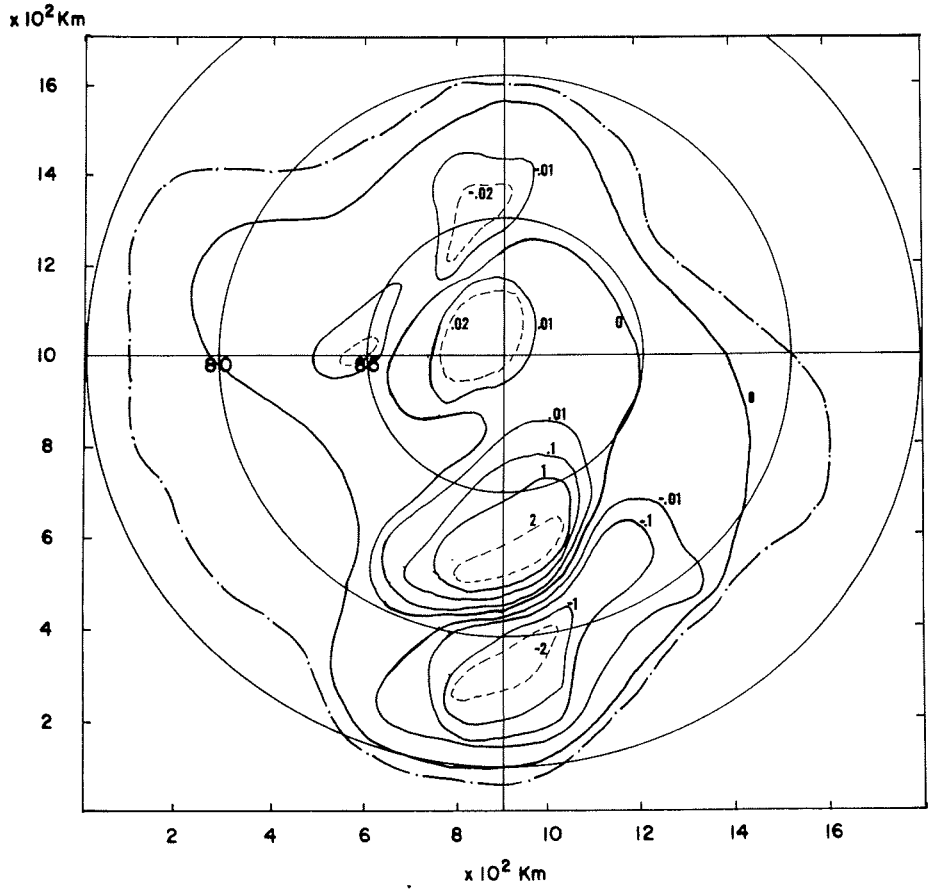

Fig. 9: Isotachs (mm a^{-1}) of the vertical velocity at the ice cap surface. These velocities equal the divergence of the volume flux (Fig. 8) and, in steady-state conditions, the rates of accumulation (>0) and ablation (<0).

Abb. 9: Linien gleicher Vertikalgeschwindigkeit (mm a^{-1}) an der Oberfläche der Eiskappe. Diese Geschwindigkeiten entsprechen der Divergenz des Massenflusses (Abb. 8) und — bei stationärem Zustand — der Akkumulations- (>0) bzw. Ablationsrate (<0).

The results can be exemplified for the cross section shown as a heavy line in Fig. 3. Its basic features are shown in Fig. 10 and some of its ice trajectories and age horizons in Fig. 11 where elevation and ice thickness have been used as alternative vertical coordinates. Numerical values are given in Tab. 1 and show that the age of the ice in the ablation zone downstream from this most active part of the ice cap is in the range of 1 to 10 Ma; elsewhere the ice is an order of magnitude older. Fig. 12 shows the isochrones constructed from the points of emergence of all the flowlines in Fig. 3 (these ages are zero inside the accumulation area, by definition). The isochrones are well separated in the regions of maximum velocity (cf. Fig. 7) but crowd together where the ice is stagnating, especially in the grid NE corner of the ice cap. It is in these regions, and also all around the outer reaches of the ice cap, that the ablation of the ice reveals the deposits of dust in the "layered terrain".

6. BASAL TEMPERATURES

As discussed in section 3, the surface elevations can be assumed to control the surface layer annual mean temperature T_s. Its isotherms have been constructed to give a slightly super-adiabatic topographical lapse

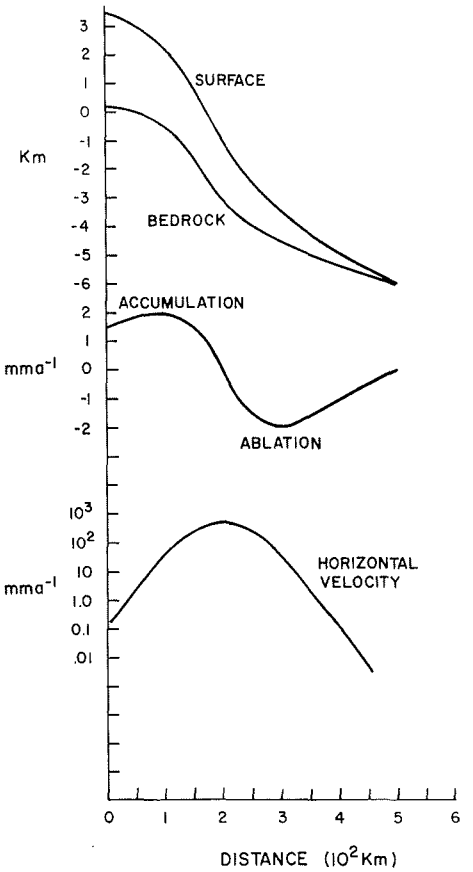

Fig. 10: Features of the cross section along the heavy line in Fig. 3.

Abb. 10: Charakteristiken des Querprofiles längs der verstärkten Linie in Abb. 3.

rate (which also includes some small latitudinal component), i. e. with

$$T_s = -80 - 5E\,^{\circ}\mathrm{C}\ (E \text{ in km}) \tag{8}$$

and are shown in Fig. 13.

The small horizontal and vertical velocities in Figs. 7 and 9 confirm that the linear solution (4) of the ther-

Trajectory #	I		II		III		IV		V		VI	
Distance (km)	Depth (km)	age (Ma)	Depth (km)	Age (Ma)	Depth (km)	Age (Ma)	Depth (km)	Age (Ma)	Depth (km)	Age (Ma)	Depth (km)	Age (Ma)
25	2.96	5.38	—	—	—	—	—	—	—	—	—	—
50	3.00	7.65	2.23	2.27	—	—	—	—	—	—	—	—
75	2.87	8.53	2.45	3.16	1.24	0.88	—	—	—	—	—	—
100	2.78	8.89	2.46'	3.51	1.54	1.24	0.61	0.35	—	—	—	—
150	2.39	9.19	2.16	3.81	1.50	1.54	0.83	0.65	0.40	0.30	—	—
200	1.99	9.32	1.81	3.95	1.28	1.67	0.74	0.79	0.39	0.44	0.07	0.14
250	1.49	9.46	1.35	4.08	0.39	1.81	0.51	0.92	0.24	0.57	—	—
300	0.99	9.89	0.81	4.52	0.30	2.24	—	—	—	—	—	—
350	0.13	12.16	—	—	—	—	—	—	—	—	—	—

Tab. 1: Particle trajectories and ages in a cross section through the North Polar ice cap of Mars.

Tab. 1: Teilchenbahnen und Alter in einem Querprofil durch die nordpolare Eiskappe des Mars.

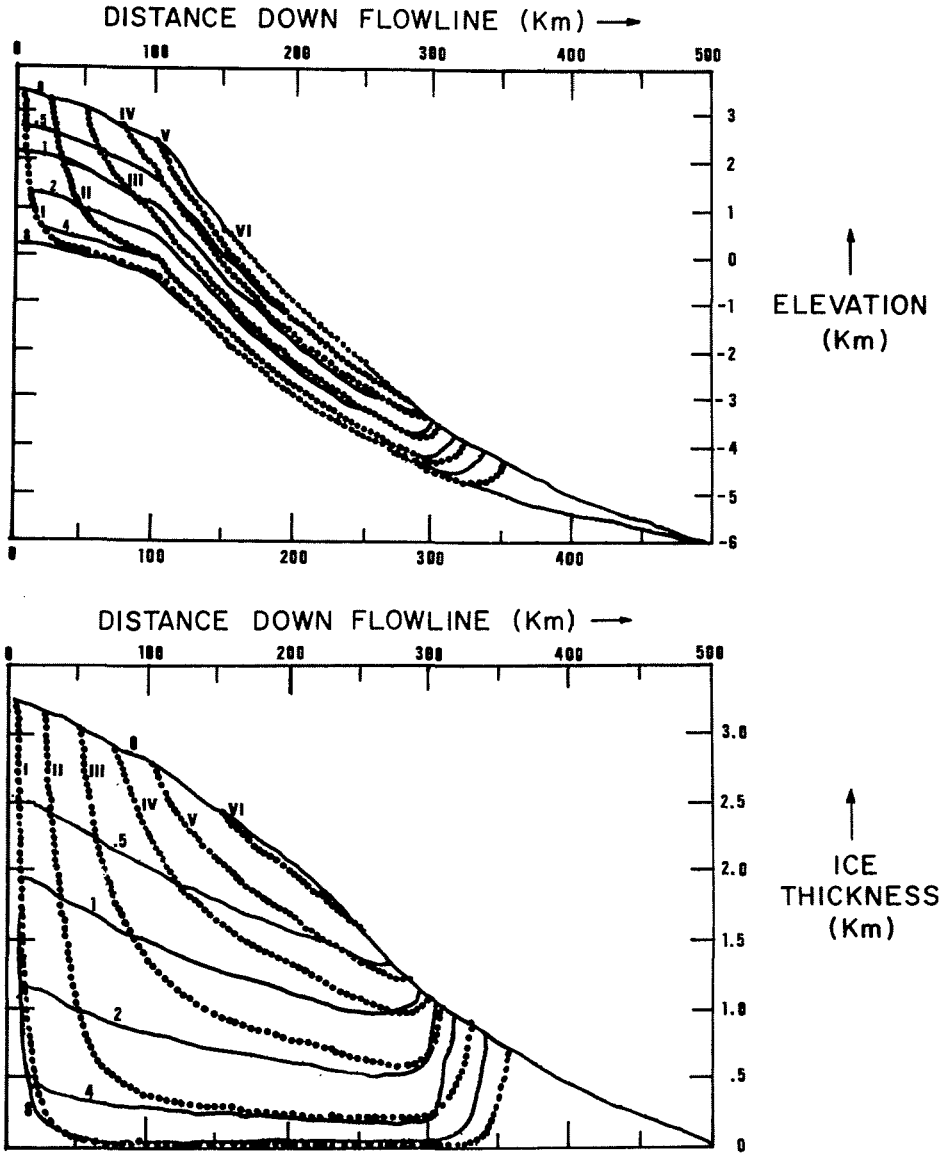

Fig. 11: Particle trajectories (dotted lines) and age horizons (Ma) in the cross section along the heavy line in Fig. 3.

Abb. 11: Teilchenbahnen (gepunktete Linien) und Altershorizonte (Ma) im Querprofil längs der verstärken Linie in Abb. 3.

modynamic equation (3') should be a valid approximation to the internal temperature distribution. Rough estimates of the temperature T_b at the base of the north polar ice cap of Mars have therefore been constructed from the surface isotherms of Fig. 13 by adding the ice thickness Z (Fig. 6) scaled with assumed "areothermal" gradients γ_a, giving

$$T_b = -80 - 5E + \gamma_a Z \tag{9}$$

Following TOKSOZ & HUI (1978) the first choice for the areothermal heat flux was $q_a = 0.8\ \mu$ cal

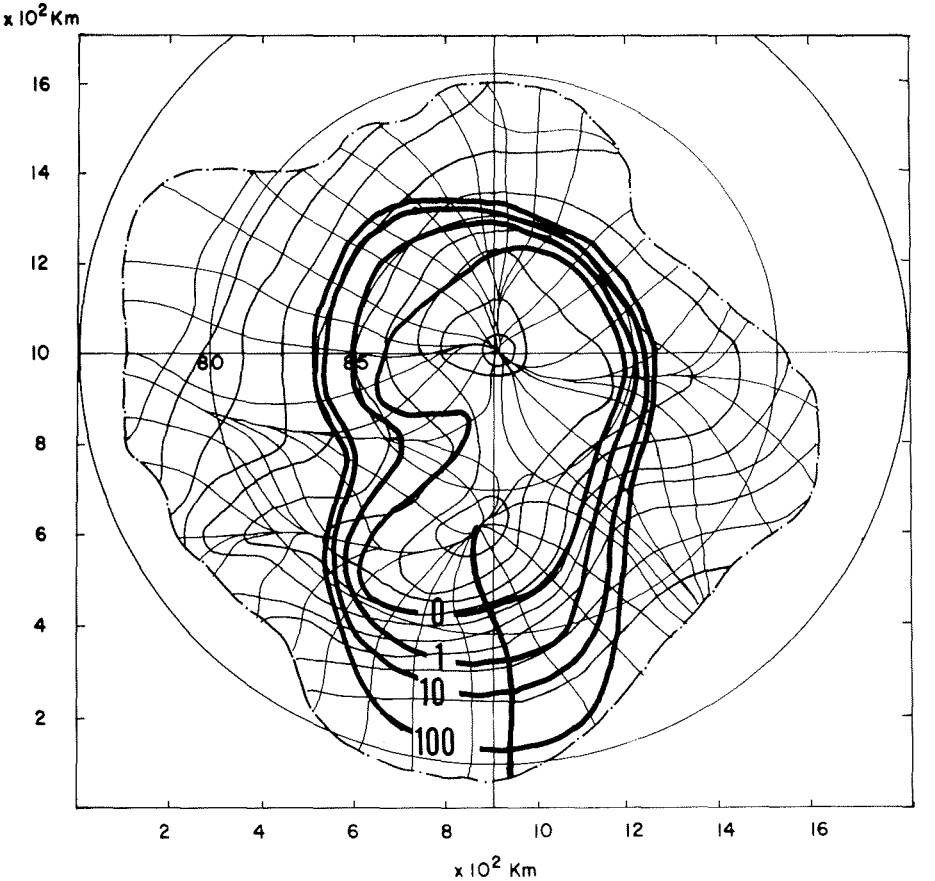

Fig. 12: Isochrones (Ma, heavy lines) of the ice emerging in the ablation area of the ice cap Thin lines: elevation contours and flowlines.

Abb. 12: Linien gleichen Alters (Ma, verstärkte Linien) des in der Ablationszone der Kappe austretenden Eises. Dünne Linien: Höhen- und Stromlinien.

$cm^{-2}s^{-1}$ giving a vertical temperature gradient $\gamma_a = \frac{q_a}{K} \approx 15\,° \text{ km}^{-1}$, with $K_{ice} = 6 \times 10^{-3}$ cal cm $^{-1}$ $C^{-1}s^{-1}$. The resulting basal temperatures are shown in Fig. 14 and are everywhere well below the pressure melting point $T_p = -0.77Z\,°C$. When q_a is doubled to equal a representative terrestrial value (1.6 μ cal, $\gamma_a \approx 30\,°$/km), Fig. 15 shows that the melting point is reached in limited areas below the two domes of the ice cap. The implied rate of melting in these areas is obtained as

$$M = k\,(\gamma_a - (T_p - T_s)Z^{-1})\varrho^{-1}L^{-1} \qquad (10)$$

where ϱ is the ice density and L the latent heat of melting. Numerically with

$T_s = -95\,°$ C, $T_p = -2.7\,°$ C, $Z = 3.5$ km, $\varrho = .91$ g cm^{-3}, $\gamma_a = 30\,°$ km^{-1} and L = 80 cal g^{-1}

$$M \approx 1 \text{ mm a}^{-1}$$

This amount has to be added in the melt regions to the previously computed surface mass balance in order to maintain the ice cap in steady state. A further increase follows from the faster ice flow implied by

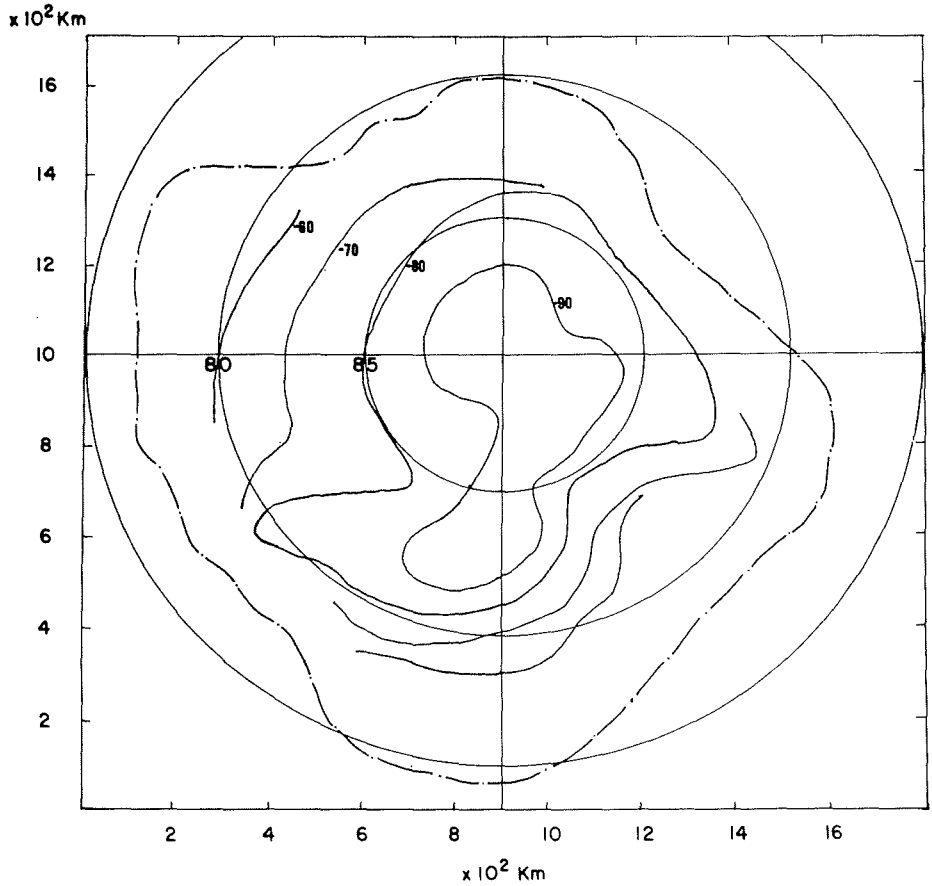

Fig. 13: Surface temperature $T_s = -80 - 5E$ (°C) constructed from Fig. 3. Large gradients have been assumed near the transition to the flat outer region of the ice cap.

Abb. 13: Isothermen der Oberfläche $T_s = -80 - 5E$ (°C), konstruiert aus Abb. 3. Nahe dem Übergang zum flachen äußeren Gebiet der Eiskappe werden starke Gradienten angenommen.

the higher temperatures of the lower ice layer. The algebraic argument in the appendix shows that raising the difference between the surface temperature T_s and the representative temperature T by 10° C increases the velocity factor k in equation (2), and hence the inferred accumulation rate needed for balance, by a factor of about 5. To these uncertainties arising from the unknown aerothermal heat flux must be added the possible errors in the estimated surface layer temperatures and ice thicknesses, so that the thermal patterns in Figs. 14 and 15 at best give orders of magnitude; however they suggest that unless the aerothermal gradient is unexpectedly large, basal melt is not a significant factor in the ice cap mass balance.

7. DISCUSSION

The basic problem here addressed can be stated as follows: could the north polar ice cap of Mars remain in an almost steady state by ice flow from a central area with net mean accumulation (of the order of a few tenths of millimeters per year of water ice), to a surrounding outer area with mean net ablation of the same order? The broad answer is that the necessary annual mass flow would be of the order of 1 to 2 m^3 ice/m and could be produced by ice 1 or 2 km thick moving at velocities around 1 mm a^{-1}. Such velocities

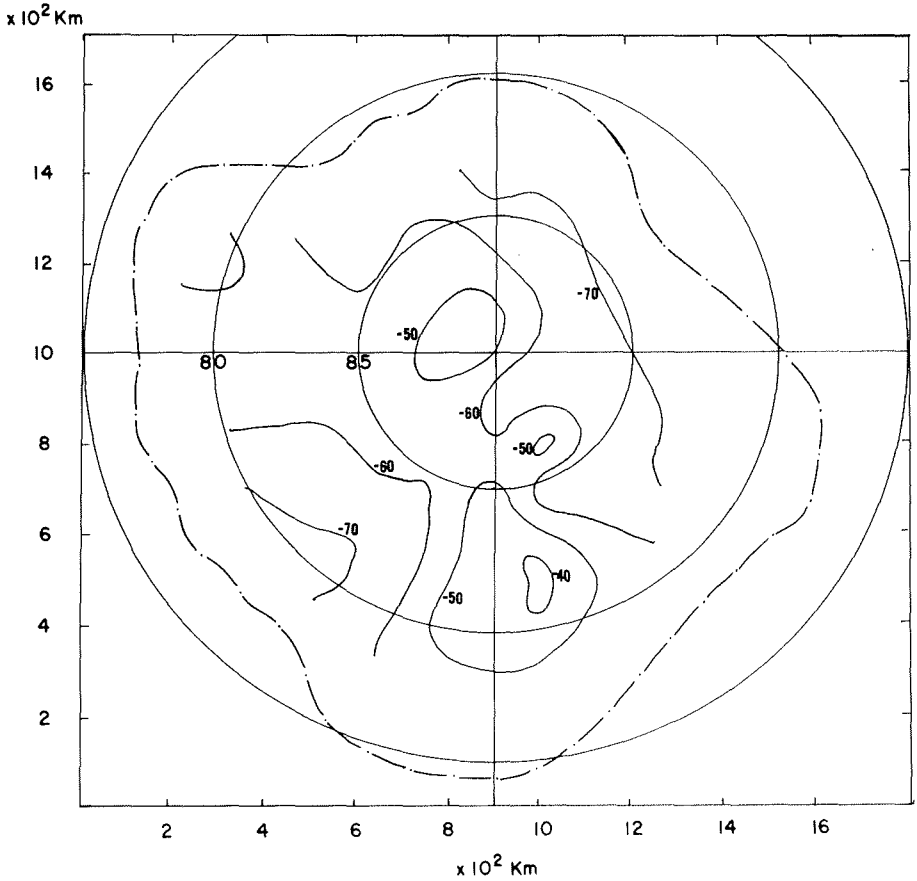

Fig. 14: Basal temperature (T_b °C) constructed from Figs. 6 (Z) and 13 (T_s) with $T_b = T_s + \gamma_a Z$ and $\gamma_a = 15°\,C\,km^{-1}$.

Abb. 14: Isothermen am Untergrund (T_b °C), konstruiert aus Abb. 6 (Z), und 13 (T_s) mit $T_b = T_s + \gamma_a Z$ und $\gamma_a = 15°\,C\,km^{-1}$.

are compatible with the stresses that could exist in a thick ice-dust deposit and with its flow properties.

The working hypothesis that the north polar ice deposit exactly balances its mass gains by ice flow and ablation then has made it possible here to estimate a number of physical quantities which are difficult or impossible to measure even on terrestrial ice sheets. It should be stressed that the order of magnitude of these estimates does not require exact balance but remains the same in the presence of the very slow changes that characterize all large ice masses. Even for the Antarctic and Greenland ice sheets it is not yet possible to point to any clear deviations from steady-state balance, despite 30 years of intensive measurements. The simulated features of the northern ice cap of Mars therefore are much less likely to be vitiated by a slightly imbalanced regime than by errors in the assumptions made for basic as yet unmeasured features.

The most crucial of these features is the thickness of the ice-dust deposit. Our assumed thickness is supported by a variety of direct and indirect evidence: the trend of the ice-free terrain surrounding the ice cap, the lateral extent of the ice, and the length of the surface undulations. The undulations and the absence of craters in the north polar region suggest rheological properties for the ice-dust deposit which are not radically different from those established by laboratory experiments on clean and dirty terrestrial ice

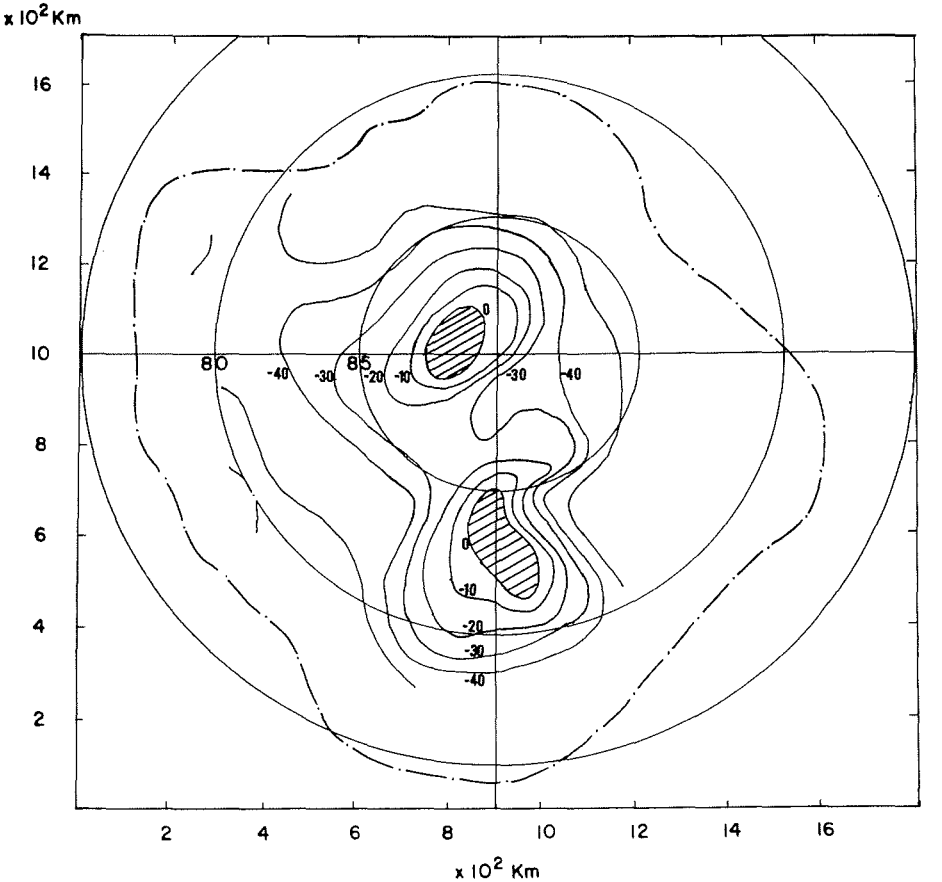

Fig. 15: Basal isotherms (T_b °C) constructed from Figs. 6 (Z) and 13 (T_s) with $T_b = T_s + \gamma_a Z$ and $\gamma_a = 30\,°\,C\,km^{-1}$. the hatched areas have the pressure-melting temperature $T_p = -0.77\ Z$ °C (Z in km).

Abb. 15: Isothermen am Untergrund (T_b °C), konstruiert aus Abb. 6 (Z) und 7 (T_s) mit $T_b = T_s + \gamma_a Z$ und $\gamma_a = 30\,°\,C\,km^{-1}$. Die schraffierten Gebiete haben die Temperatur des Druckschmelzpunktes $T_p = -0.77\ Z$ °C (Z in km).

(HOOKE et al., 1972, 1980; RUSSELL-HEAD & BUDD, 1979; LILE, 1984). The modelled accumulation area closely agrees in extent with that of the residual clean ice at the end of summer. Finally calculated rates of accumulation and ablation are similar to those previously inferred by other means and implicitly lend credence to the calculated ice velocities.

The consistency of these results provides support for the views that the north polar ice cap of Mars indeed has physical features resembling those of the medium-sized terrestrial ice sheets. Its true thickness awaits direct seismic or radar measurements; clearly a large mass of water ice would help to account for the many morphological features suggesting floods and large bodies of water on Mars in earlier times.

8. CONCLUSION AND OUTLOOK

The order of magnitude of the ages suggested by our analysis for the deeper ice and the outer reaches of the ice cap shows that these must be remnants of earlier ice cap configurations which presumably were substantially different from the present one. Such earlier ice caps have been postulated to explain the wi-

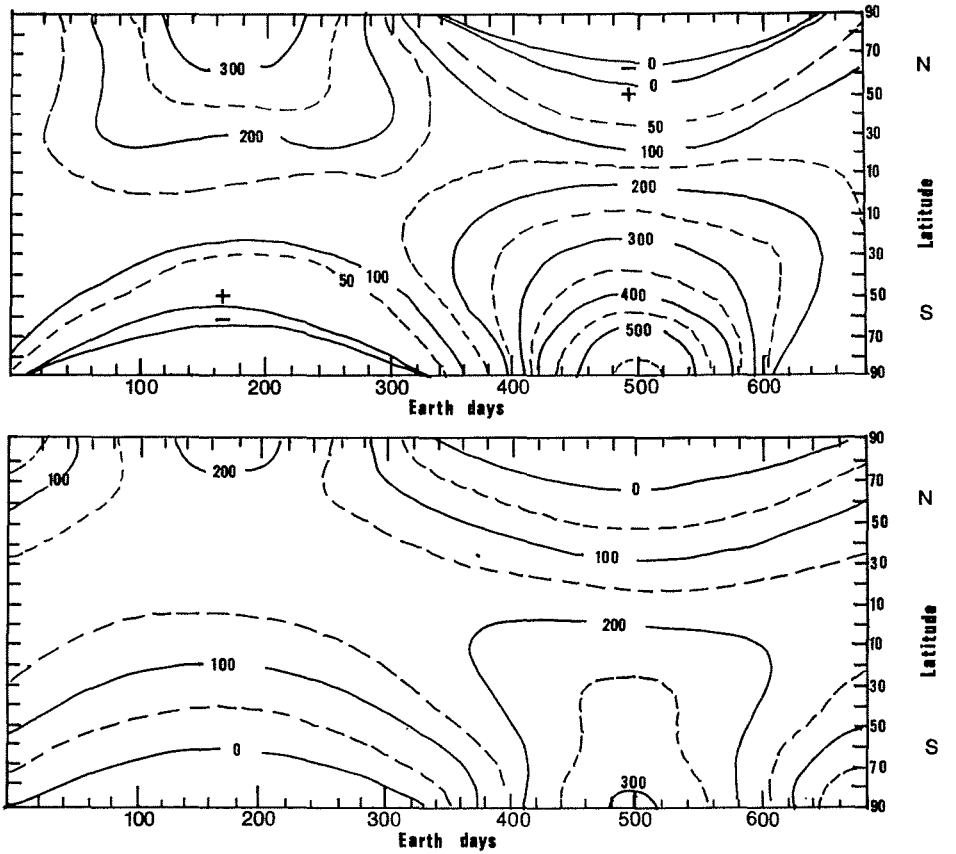

Fig. 16: Daily radiation intake (W m^{-2}) of different latitudes during a Mars year. Bottom: Insolation for the present obliquity $\epsilon = 25°$. Top: Increase in insolation for $\epsilon = 35°$.

Abb. 16: Tägliche Sonneneinstrahlung (W m^{-2}) in verschiedenen geographischen Breiten während eines Marsjahres. Unten: Sonneneinstrahlung bei der derzeitigen Achsschiefe $\epsilon = 25°$. Oben: Zunahme der Sonneneinstrahlung für $\epsilon = 35°$.

de extent of the layered terrain on the Martian surface and could be reconstructed with a time-dependent ice sheet model similar to that used by BUDD & SMITH (1981, 1987) to simulate the North American ice sheets of the past 500.000 years. This could require coupling the ice flow model to an energy balance model which can simulate the range of Martian climates resulting from the orbitally varying radiation regimes of Mars. These regimes are represented in Fig. 16 by the current daily radiation intake and by the changes corresponding to a 10° increase in obliquity from 25° to 35°. At the high obliquity stage the north polar region in midsummer receives 70% more radiation than at present, and the south polar region almost twice as much as now, while only a narrow latitude band in the winter hemisphere is receiving less. The implication is that from the present large deposit of north polar ice (here estimated as $10^6 km^3$) a large melt pool could have been created under the ice by the warmer climate of the past. In transition periods "Jøkulaup"-type flood outbursts could have happened, explaining the apparent flood terrain described by BAKER (1982).

Such inferences clearly stretch the available data to or beyond their limits. The model results here presented can however serve as a starting point and as pointers to firmer conclusions that will become possible as further Viking observations are evaluated and new observations flow from future missions to Mars.

APPENDIX: Determination of the Mars Velocity and Mass Balance

The continuity equation along a flowline, in the absence of basal melt, is

$$\frac{\delta Z}{\delta t} + \nabla\cdot(VZ) = A$$

where V is the vector flowline velocity, Z is ice thickness, and A is accumulation. For steady state

$$\delta Z/\delta t = 0 \text{ and } A = \nabla\cdot(VZ)$$

or

$$A = \frac{\delta(uZ)}{\delta x} + \frac{\delta(vZ)}{\delta y} \tag{1}$$

where u and v are the components of the velocity in the x and y direction. It is assumed that the flow is down the gradient of elevation, E. so

$$u = -(V/\alpha)\frac{\delta E}{\delta y}$$

$$v = -(V/\alpha)\frac{\delta E}{\delta y}$$

where α, the surface slope, is

$$\alpha = \left[\left(\delta E/\delta x\right)^2 + \left(\delta E/\delta y\right)^2\right]^{1/2} \tag{2}$$

Now define β as

$$\beta = -VZ/\alpha.$$

so that equation (1) becomes:

$$A = \frac{\delta}{\delta x}\left(\beta\frac{\delta E}{\delta x}\right) + \frac{\delta}{\delta y}\left(\beta\frac{\delta E}{\delta y}\right) \tag{3}$$

This equation gives the mass balance at any point from the known or computed values of velocity (V), ice thickness (Z) and surface slope (α), found from E by equation (2).

The velocity is given by a power flow relation:
$V = k(\varrho g\alpha Z)^3 Z$
where k (units of $bar^{-3}\ yr^{-1}$) is:
$k = 0.01\ 10^{(T_s+20)/15} = \exp.\ [0.1535056\ (T_s-10)]$
where T_s is the surface temperature.
Since, for elevation E in km, $T_s \approx$ -80-5E, k becomes
$k = \exp\ [-13.815504 - 0.76753283E + \gamma Z]$
Also, for Z in km,
$\varrho g\alpha Z = 918 \times 3.73 \times (1000Z)\alpha \times 10^{-5}$* $= 34.2414\ \alpha Z$ bar. Hence

$$V = 4.0147133 \times 10^7\ \alpha^3 Z^4 \exp\ [-13.815504 - 0.765282E) \quad \text{m yr}^{-1} \tag{4}$$

where Z and E are in km. Finally, then

$$\beta = -4.014733 \times 10^7\ \alpha^3\ Z^5 \exp\ [-13.815504 - 0.765283E)$$

* 1 bar = 10^5Pa

References

Baker, V. R. (1982): The channels of Mars. — Helger.

Blasius, K. R., Cutts, J. A. & A. D. Howard (1982): Topography and stratigraphy of Martian polar layered deposits. — Icarus 50: 140—160.

Budd, W. F. (1970): Ice flow over bedrock perturbations. — J. Glaciol. 9 (55): 19—28.

Budd, W. F. & D. B. Carter (1971): An analysis of the relation between the surface and bedrock profiles of ice caps. — J. Glaciol. 10: 197—209.

Budd, W. F., Jenssen, D. & U. Radok (1970): The extent of basal melting in Antarctica. — Polarforschung 39: 293—306.

Budd, W. F., Young, N. W. & C. R. Austin (1976): Measured and computed temperature distributions in the Law Dome Ice Cap, Antarctica. — J. Glaciol. 16: 99—109.

Budd, W. F. & I. N. Smith (1981): The growth and retreat of ice sheets in response to orbital radiation changes. — Intern. Ass. Hydrol. Sci. Publ. 131: 369—409.

Budd, W. F. & I. N. Smith (1987): Conditions for growth and retreat of the Laurentide ice sheet — Paper to be presented to the INQUA Laurentide Ice Sheet Symposium.

Budd, W. F. & N. W. Young (1979): Results from the I. A. G. P. flow-line study inland of Casey, Wilkes Land, Antarctica. — J. Glaciol. 24, 89—101.

Cutts, J. A., Blasius, K. R. & W. J. Roberts (1979): Evolution of Martian polar landscapes: Interplay of long-term variations in perennial ice cover and dust storm intensity. — J. Geophys. Res. 84 (86), 2975—2994.

Cutts, J. A. & B. H. Lewis (1982): Model of climate cycles recorded in Martian polar layered deposits. — Icarus 50: 216—244.

Dzurisin, D. & K. R. Blasius (1975): Topography of the polar layered deposits of Mars. — J. Geophys. Res. 80 (23): 3286—3306.

Farmer, C. B. & P. E. Doms (1979): Global seasonal variations of water vapor on Mars and the implications for permafrost. — J. Geophys. Res. 84: 2881—2888.

Goody, R. M. & J. C. G. Walker (1972): Atmospheres. — Prentice-Hall

Hooke, R. LeB., Dahlin, B. B. & M. T. Kauper (1972): Creep of ice containing dispersed fine sand. — J. Glaciol. 11 (63): 327—336.

Hooke, R. LeB., Mellor, M., Budd, W. F., Glen, J. W., Higashi, A., Jacka, T. H., Jones, S. J., Lile, R. C., Martin, R. T., Meier, M. R., Russell-Head, D. S., & J. Weertman (1980): Mechanical properties of polycrystalline ice: An assessment of current knowledge and priorities for research. Report prepared for the International Commission on Snow and Ice, with support from the U. S. National Science Foundation. — Cold Regions Science and Technology 3: 263—275.

Howard, A. D., Cutts, J. A. & K. R. Blasius (1982): Stratographic relationships within Martian polar cap deposits. — Icarus 50: 161—215.

Jakosky, B. M. & C. B. Farmer (1982): The seasonal and global behavior of water vapor in the Mars atmosphere: Complete global results of the Viking Atmospheric Water Detector Experiment. — J. Geophys. Res. 87 (84): 2999—3019.

Jenssen, D. & U. Radok (1982): On the joint interpretation of total gas contents and stable isotopes ratios in ice cores. — Annals of Glaciol. 3: 152—155.

Kieffer, H. H., Martin, T. Z., Peterfreun, A. R., Jakosky, B. M., Miner, E. D. & F. D. Palluconi (1977): Thermal and albedo mapping during the Viking primary mission. — J. Geophys. Res. 78: 4291—4312.

Kondratyev, K. Y. & G. E. Hunt (1982): Weather and Climate on Planets. — Pergamon.

Krass, M. S. (1983): Matematicheskaya teoriya glyatsiomekhaniki (Mathematical theory of glacier mechanics — Moscow, Vsesoyuzhnyy Institut Nauchnoy i Teknicheskoy Informatsii. (Itogi Nauki. Seriya Glyatsiologiya, 3.)

Krass, M. W. (1985): Ice on planets of the solar system. — J. Glaciol 30 (106): 259—274.

Lile, R. C. (1984): The flow law for isotropic and anisotropic ice at low strain rates. — ANARE Report 132, Canberra.

Malin, M. C. (1986): Density of Martian north polar layered deposits: Implications for composition. — Geophys. Res. Lett. 13: 444—447.

Pollack, J. B., Colburn, D. S., Flasar, F. M., Kahn, R., Carlston, C. E. & D. Pidek (1979): Properties and effects of dust particles suspended in the Martian atmosphere. — J. Geophys Res. 84, 2919—2945.

Pollack, J. B. & O. B. Toon (1982): Quasi-periodic climate changes on Mars: A review. — Icarus 50: 259—287.

Russell-Head, D. S. & W. F. Budd (1979): Ice sheet flow properties derived from borehole shear measurements combined with ice core studies. — J. Glaciol. 24 (90): 117—130.

Toksoz, M. N. & A. T. Hui (1978): Thermal history and evolution of Mars. — Icarus 34: 537—547.

Toon, O. B., Pollack, J. B., Ward, W. R., Burns, J. A. & K. Bilski (1980): The astronomical theory of climatic change on Mars. — Icarus 44: 552—607.

Ward, W. B. (1974): Climatic variations on Mars: I. Astronomical theory of insolation. — J. Geophys. Res. 79: 3375—3386.

Weertman, J. (1976): Milankovich solar radiation variations and ice age ice sheet sizes. — Nature 261: 17—20.